

InP Microdisk Lasers Integrated on Si for Optical Interconnects

Geert Morthier, *Senior Member, IEEE*, Thijs Spuesens, *Member, IEEE*, Pauline Mechet, Gunther Roelkens, *Member, IEEE*, and Dries Van Thourhout, *Member, IEEE*

(Invited Paper)

Abstract—We review recent theoretical and experimental work on InP membrane microdisk lasers heterogeneously integrated on SOI and coupled to a Si bus waveguide. The lasers can now be fabricated with very high yield, have typical threshold currents of 0.5 mA and output powers of tens of μW , while the total power consumption is restricted to 5 mW. First, we describe various improvements in the fabrication technology and interesting results on the uniformity in device characteristics. In a second part, unidirectional behaviour and reflection sensitivity are briefly discussed. The third part is focused on optical signal regeneration with microdisk lasers. The last part contains a brief summary of optical interconnects based on heterogeneously integrated microdisk lasers and heterogeneously integrated photodetectors.

Index Terms—Silicon photonics, microdisk lasers, optical interconnect, heterogeneous integration.

I. INTRODUCTION

HETEROGENEOUSLY integrated microdisk lasers have been studied since a decade [1] and were among the first electrically pumped InP lasers integrated on silicon. Because of the high optical confinement in the InP membranes, the small disk diameters (10 μm or lower) and the weak, evanescent coupling to the underlying Si bus waveguide, such microdisk lasers can have relatively low threshold gain and threshold current and are therefore rather well suited as sources for optical interconnects [2], [3]. This is especially relevant as silicon photonics is considered more and more as the platform in which to implement optical interconnects [4].

While photonic crystal lasers are known to exhibit lower thresholds, the difficulty in pumping them electrically and their very weak output powers make them so far less suitable for such applications, unless transmission losses are extremely low [5]. Off-chip light sources on the other hand are more difficult to use with complex interconnect networks [6].

Heterogeneously integrated microdisk lasers (see Fig. 1) make use of the high optical confinement that can be obtained in a thin (0.6 μm) bonded InP membrane. A centrally located

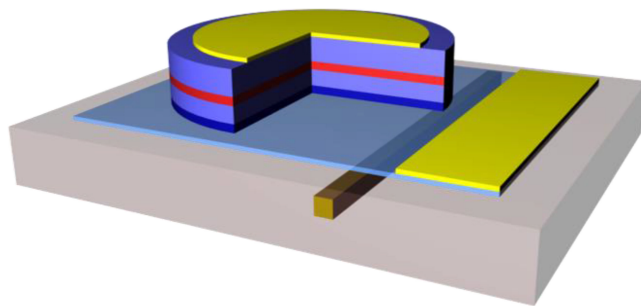


Fig. 1. Schematic view of an InP microdisk laser heterogeneously integrated onto SOI.

top contact on this thin membrane furthermore allows a whispering gallery mode with low loss, while giving high loss for all other modes. Heterogeneously integrated microdisk lasers are relatively easy to incorporate in silicon photonic integrated circuits. Indeed, ring or disk lasers don't require reflecting facets or diffraction gratings and are relatively easy to fabricate. As will be discussed further on, they can be configured to lase in a predefined unidirectional mode and to be less sensitive to external reflections [7]–[9].

The typical threshold current of our microdisk lasers is around 0.5 mA, with an output power at 5 mA up to a few hundreds of μW (in the silicon waveguide) and total power consumption of a few mW [10]. The free spectral range of the microdisk resonator for a diameter of 7.5 μm is slightly over 30 nm, giving the lasers a stable single mode behavior with a side mode suppression over 40 dB. For a 7.5 μm diameter CW-operated microdisk, a minimum threshold current of 0.22 mA and a maximum single-sided slope efficiency of 57 $\mu\text{W}/\text{mA}$ have been observed [11].

Microdisk and ring lasers have also been studied extensively in the past decade, because of their suitability as bistable lasers for optical switching or signal processing applications such as all-optical flip-flops, gates and wavelength converters [10], [12]–[16].

Several improvements in the fabrication technology have been successfully implemented in recent years. This has led to bonding yields of nearly 100% [17] and very good uniformity in the lasing characteristics of microdisk lasers fabricated on the same SOI die [18]. In addition to the bonding, there are a number of other aspects which require special attention though (see Fig. 1):

- Overlap of the top contact with the whispering gallery mode must be avoided, as this leads to excess loss with the very thin (0.5 μm) membranes used.

Manuscript received September 29, 2014; revised November 24, 2014; accepted November 24, 2014. This work was supported in part by the European FP7 project HISTORIC.

The authors are with the Photonics Research Group, Department of Information Technology, Ghent University—IMEC, B-9000 Gent, Belgium (e-mail: morthier@intec.ugent.be; Thijs.Spuesens@intec.ugent.be; pauline.mechet@intec.ugent.be; gunther.roelkens@intec.ugent.be; dries.vanhourhout@intec.ugent.be).

Color versions of one or more of the figures in this paper are available online at <http://ieeexplore.ieee.org>.

Digital Object Identifier 10.1109/JSTQE.2014.2376697

- Careful alignment of the microdisks with the underlying silicon wire waveguide to obtain optimum coupling
- The small volume of the membrane and its adhesive bonding onto SOI give rather poor heat sinking.

Fabrication and design have been optimized to account for these potential problems and this is explained in more detail in the first part of this paper.

For optical interconnect even more than for long distance communications, high efficiency and isolator-free operation of light sources are of paramount importance. Some theoretical and experimental work has therefore been dedicated to unidirectional operation (in a predefined direction) and to the feedback sensitivity of the microdisk lasers and it is the subject of the second part of this paper.

Asymmetrically terminated ring or disk lasers, which are necessary for unidirectional operation, also lend themselves very well for low-power optical signal regeneration. Integration of such a microdisk laser with a photodiode could actually serve as a regenerative receiver with low power consumption. We will briefly summarize the results obtained so far on this 2R regeneration (2R = Re-amplification and Reshaping) in the third part.

The fourth and last part gives an account of some system experiments using both heterogeneously integrated lasers and heterogeneously integrated detectors. The interconnect links that are proposed in this part can be completely fabricated in a CMOS pilot line.

II. DESIGN AND FABRICATION

Optimised designs of microdisk lasers are aimed towards minimizing the cavity losses. The internal loss consists of bend losses, scattering loss due to surface wall roughness, intervalence band absorption (IVBA) in p-doped contact layers and losses due to overlap of the whispering gallery mode with the top metal contact. Scattering loss is minimized by utilizing optimized inductively coupled plasma etching, while IVBA has so far been limited by the incorporation of a tunnel junction in the epitaxial structure to avoid heavily p-doped regions.

Bend losses decrease with increasing disk radius and depend also on the thickness of the bottom contact layer. However, at least for disk radii beyond $3\ \mu\text{m}$, the loss is dominated by other factors [19]. Microdisk lasers with diameters beyond $10\ \mu\text{m}$ (e.g., 20 and $40\ \mu\text{m}$) have so far not given higher output powers than those with diameters of 7.5 and $10\ \mu\text{m}$, but they have higher threshold current and can be multi mode. The threshold current density was generally found to be fairly constant for disk diameters above $8\ \mu\text{m}$, but increase for smaller diameters due to increased bend and scattering losses [20].

To avoid large threshold currents, the coupling loss (or facet loss) should not be much larger than the internal loss, while it should also not be much smaller than the internal loss to guarantee a sufficient external efficiency.

The coupling between the microdisk's whispering gallery mode and the underlying silicon waveguide relies on evanescent coupling and depends on the thickness of the bonding layer, the width of the silicon waveguide and the alignment between silicon waveguide and microdisk. The width of the Si waveguide

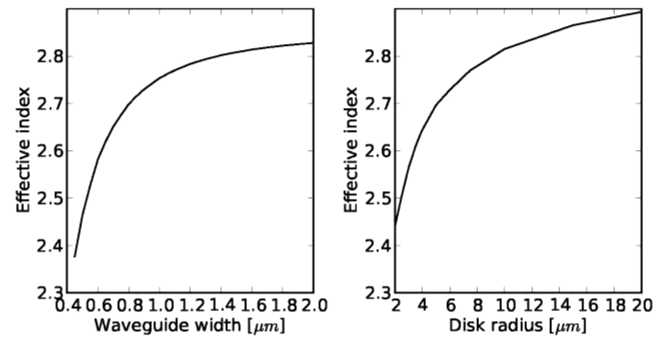


Fig. 2. (a) Effective index of the fundamental mode in a 220 nm thick silicon waveguide versus waveguide width. (b) Effective index for azimuthal propagation of the fundamental mode in a 580 nm thick microdisk versus disk radius.

is chosen so as to obtain phase matching with the microdisk mode. Fig. 2 shows simulated values for the effective index of the fundamental mode of both a 220 nm Si waveguide with variable width and a 580 nm thick microdisk with variable radius R [20]. The effective index considered for the microdisk mode is that for the (azimuthal) propagation along the disk perimeter. The values were obtained assuming that the maximum mode intensity is obtained at the disk radius R and they are therefore lower limits. If a microdisk radius of $3.5\ \mu\text{m}$ is considered, a Si waveguide width of slightly over 600 nm gives the best phase matching.

The alignment of the disk with respect to the Si waveguide must be chosen so as to maximize the coupling between the fundamental disk mode and the fundamental waveguide mode and to minimize the coupling between the fundamental disk mode and higher order (leaky) waveguide modes (and vice versa). Simulation results indicate that a waveguide width of 800 nm is even better for this purpose and that the optimum offset of 300 nm away from the waveguide middle gives the least parasitic coupling.

The bonding of the InP dies to the SOI dies can be done using direct [21], molecular (silica to silica) bonding [22] and adhesive bonding [23]. Direct and molecular bonding allow much better heat dissipation than adhesive bonding, as the thermal conductivity of the adhesive used for bonding is rather poor. However, they also require a much better wafer quality (in terms of roughness, defects, etc.). On the other hand, adhesive bonding layers can be widely varied in thickness, from 20 nm to $2\ \mu\text{m}$.

In the case of adhesive bonding, DVS-BCB (divinylsiloxane-benzocyclobutene) is used as adhesive, which is also used to planarize the SOI die. DVS-BCB reportedly has marginal adhesion to III-V semiconductors, so it was decided to employ an intermediate silica (or alumina) layer deposited on the InP prior to bonding. Moreover, using a controllable thickness for the silica (or alumina) and a very thin DVS-BCB layer (e.g., 30 nm) allows much better control of the total bonding layer thickness since only the relative BCB layer thickness can be controlled well. Silica (and even more alumina) are also better thermal conductors than DVS-BCB. Bonding with a rather thick oxide layer and a thin DVS-BCB layer thus gives improved heat sinking [24]. To improve the uniformity and reproducibility of the

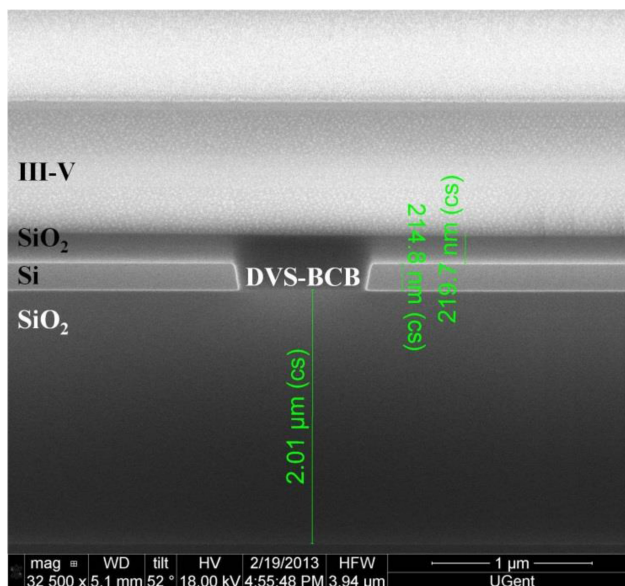


Fig. 3. FIB cross-section of a device where a 100 nm thick SiO₂ layer has been deposited prior to bonding with the wafer bonder. The measured total bonding thickness is 220 nm and the DVS-BCB layer thickness is 120 nm.

bonding layer, an optimum solution of DVS-BCB:mesitylene has been sought and with the proportions 2:3 a uniform bonding layer was obtained, without any air trapping for a SOI die with air clad waveguides [24].

Machine bonding instead of manual bonding gave further improvements in the bonding yield, uniformity and reproducibility [25]. In this case, very thin bonding layers of 35 nm can be obtained using a DVS-BCB:mesitylene dilution of 1:8 (v/v) and spin-coating at 3000 r/min. Bonding yields are now well over 90% and close to 100%. In the case of machine bonding, the BCB is precured before bonding on a hot plate for 15 min at 180 °C. The bonded samples are for both machine and manual bonding further cured under an N₂ flow, with temperatures slowly being increased to 280 °C. The dies are kept at this temperature for one hour and are then slowly cooled down to room temperature. Fig. 3 is a SEM image of a sample where 100 nm of SiO₂ has been deposited on the III–V prior to bonding and for which the DVS-BCB bonding layer is 120 nm (obtained with the 2:3 dilution).

The small volume of the microdisk lasers and the bad thermal conductivity of the DVS-BCB and the buried oxide imply a rather bad heat sinking for the laser. The thermal roll-over of microdisk lasers is therefore typically occurring at currents of a few mA. Attention has therefore been paid to a reduction of the heating as well as to an improvement of the heat sinking. The latter can be obtained among others by using a somewhat thicker bottom contact InP layer and an overcladding with oxide instead of BCB. We also employed a thick gold layer, which serves as heat sink, as part of the top contact. Finally, addition of diamond nanoparticles to the BCB bonding adhesive has proven to improve the heat flow as well [26].

A reduction of the heating itself requires reducing the optical loss and improving the efficiency of the laser. This requires

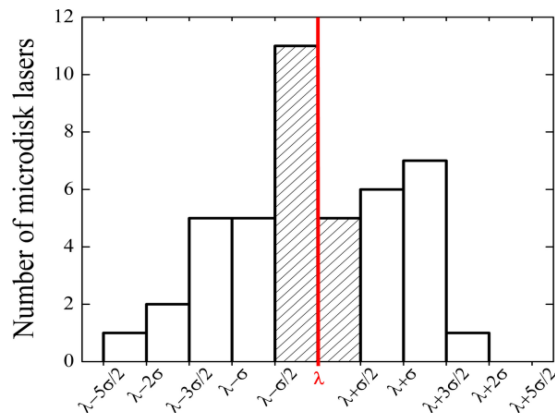


Fig. 4. Wavelength distribution of 43 microdisk lasers from the same sample centered on λ . The patterned area shows that the peak lasing wavelength of 16 microdisk lasers is between $\lambda-\sigma/2$ and $\lambda+\sigma/2$ (with $\sigma = 500$ pm).

optimum alignment of the top contact to avoid any overlap of the whispering gallery mode with the top contact to lower optical losses and optimum alignment of the microdisk laser with the underlying silicon wire to ensure an efficient coupling.

Increasing the bottom contact InP layer thickness from 90 to 130 nm also substantially decreased the series resistance. Optimisation of the bottom contact layer thickness and of the contact recipe led to a decrease of the series resistance from 1 k Ω to 150 Ω . The confinement of the whispering gallery mode was practically unaffected by an increase in bottom contact layer thickness.

E-beam lithography recipes have been developed to optimize the alignment of both the microdisk with respect to the underlying waveguide and the top contact with respect to the microdisk [27]. Markers for the alignment of the microdisk with respect to the Si waveguide are defined on the SOI with a resolution of 20 nm. The microdisk and the top contacts were defined with a 2.5 nm resolution. The accuracy of the alignment of the microdisk lasers with respect to the silicon waveguides was found to be better than 40 nm.

In addition to improved top contact alignment and improved disk versus Si waveguide alignment, use of this lithography also resulted in a much better uniformity of the dimensions and characteristics of microdisk lasers. In [18], a standard deviation in lasing wavelength of nominally identical devices on the same SOI die lower than 500 pm has been reported. The deviation in the diameter of the microdisks as low as a few nanometers makes all-optical signal processing applications requiring cascadedness possible.

Fig. 4 illustrates the uniformity in lasing wavelength characteristics obtained from 43 microdisk lasers fabricated on a same SOI die. This variation is small enough to allow aligning all laser wavelengths with just a few mW of thermal tuning. Such thermal tuning can be implemented using InP heaters configured as rings around the microdisks [3].

An optimum alignment of the top contact is also possible without the use of e-beam lithography, by using a ring shaped nitride hard mask instead of a disk shaped hard mask. Fig. 5

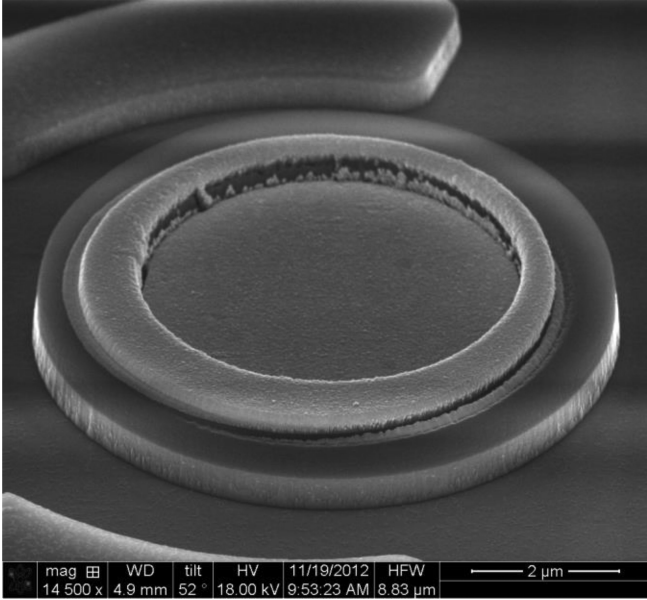


Fig. 5. SEM image of an etched microdisk with a self aligned top contact. It can be seen that the Titanium-gold metal itself is misaligned, but the metal area that contacts the disk is perfectly in the center thanks to the nitride ring.

illustrates how this hard mask leads to a self-aligned top contact even with a misalignment in the metal deposition. [8]

A last issue concerns the epitaxial III–V layer structure. So far, almost all fabricated microdisk lasers made use of a III–V epitaxial structure with a tunnel junction. This tunnel junction (consisting of two 20 nm thick, heavily doped Q1.2 InGaAsP layers) was at first considered necessary to avoid the strong absorption in the $p++$ InGaAs contact layer. The InP membrane is only about 600 nm thick and the mode profile of the whispering gallery mode extends to the top of the InP structure.

Recently, some studies were carried out with a normal p-i-n layer stack, in which the top $p++$ InGaAs contact layer is etched away at the edges of the disk to avoid overlap of the whispering gallery mode with this absorbing layer. This is illustrated in Fig. 6, where the cross section of the microdisk is shown with the regular tunnel junction containing epitaxial structure as well as with a regular pin junction. Etching the highly absorbing contact layer at the edges results in a whispering gallery mode that is still confined to the membrane and that does not overlap with the highly absorbing $p++$ InGaAs contact layer. Since the tunnel junction itself also causes significant losses for the mode, the pin structure is expected to result in lower loss for the lasing mode. Numerical simulations confirm the lower modal loss and indicate that the carrier injection efficiency into the active layer is similar as in the structure with tunnel junction.

Fig. 7 shows the calculated whispering gallery mode for the original InP structure with thin bottom contact layer (a) and for the same InP structure with thicker bottom contact layer and etched to below the tunnel junction at the edge (b).

Both increasing the thickness of the bottom contact layer and etching away the edge in the top contact and tunnel junction

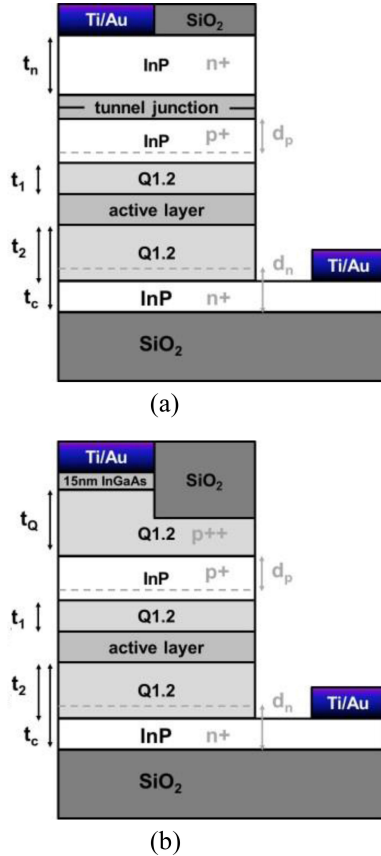


Fig. 6. Schematic structure of the InP microdisk structure for two alternative epitaxial layer stacks: (a) with the epi-layer structure including a tunnel junction, (b) layer structure with a regular pin junction, of which the highly absorbing contact layers are etched away at the edge.

layers have little effect on the mode confinement, the bend loss and on the overlap of the mode with the quantum wells. The microdisk diameter was taken as $7.5 \mu\text{m}$.

The active layer used in these simulations and in the fabricated devices consists of an SCH-MQW structure, consisting of three 6 nm thick InAsP wells, three 15 nm thick Q1.2 InGaAsP barriers and 25 nm Q1.2 InGaAsP separate confinement layers. The InP wafers were grown by molecular beam epitaxy at INL, France [28]. InAsP quantum wells are believed to show lower surface recombination than InGaAsP quantum wells [29].

III. UNIDIRECTIONALITY AND REFLECTION SENSITIVITY

To keep both cost and complexity low, efficient and isolator-free operation are of great importance for light sources for optical interconnects. Bistable unidirectional operation has been studied intensively for ring and disk lasers [7], [30] and can potentially be used in optical logic. In optical interconnect though, monostable unidirectional operation is required to maximize the external efficiency of the transmitters.

Such unidirectional behaviour has been reported before [10], [11] and has recently been analysed theoretically [9]. Unidirectional behaviour is easily obtained if the coupling

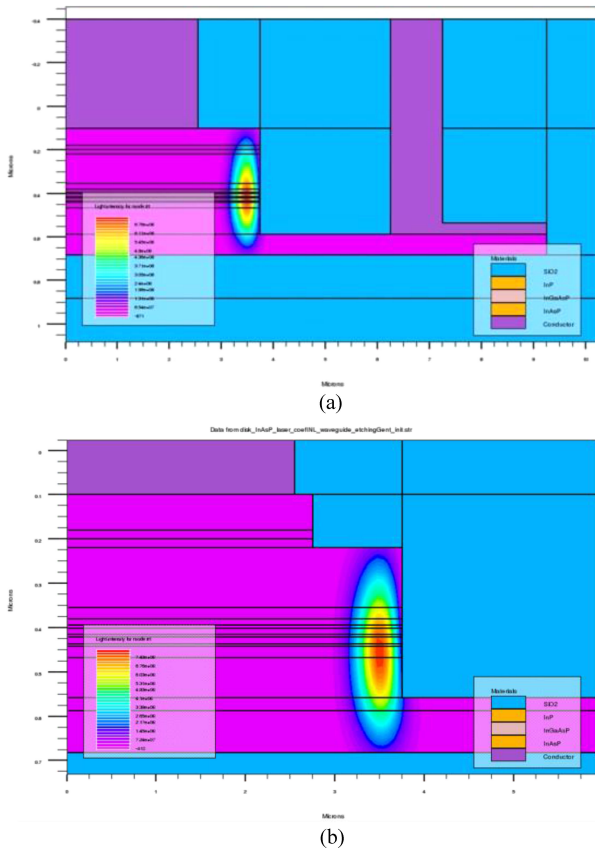


Fig. 7. Fundamental mode profile of the whispering gallery mode in the microdisk structure with (a) thin bottom contact layer and unetched top layers and (b) thicker bottom contact layer and etched top layers.

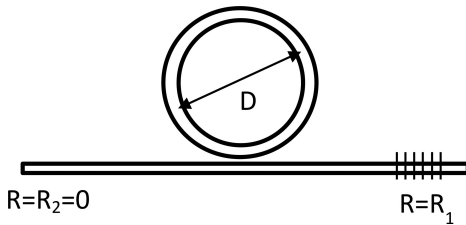


Fig. 8. Schematic structure of a ring/disk laser coupled to a bus waveguide, containing a reflector on one side.

between the CW and the CCW mode is different from the coupling between the CCW and CW mode, e.g., if the microdisk laser is coupled to a bus waveguide which has strong reflection on one side and weak reflection at the other side, as in Fig. 8. Lasing is then mainly in the direction which encounters the smallest reflection. For ease of reading and notation, we will assume that this is the CW direction.

In [11], unidirectional operation was observed in microdisk lasers with $7.5 \mu\text{m}$ diameter, coupled to a silicon bus waveguide that had a strong Bragg reflector (50 periods of 300 nm each) on one side, designed at $55 \mu\text{m}$ from the microdisk-bus coupler. Output power on both sides was measured versus bias current and versus wavelength and the result is shown in Fig. 9 for

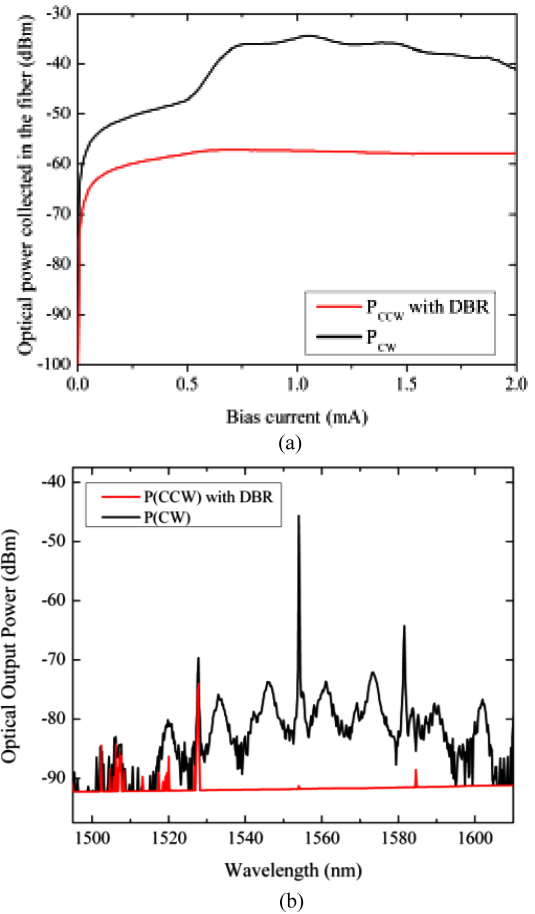


Fig. 9. L - I characteristics (top) and spectrum at 1.2 mA (bottom) of a microdisk laser coupled to a waveguide with a Bragg grating on one side. The optical power is the power collected in optical fibers on both sides of the waveguide.

a particular microdisk laser. At the peak lasing wavelength, the extinction ratio of the optical powers coupled out of the waveguide on the side of the DBR structure and on the side without the DBR is 46.1 dB . The transmission of the DBRs was derived from measurements on nominally identical SOI designs, covered in DVS-BCB and was found to be -38 dB . The 46.1 dB extinction found on the spectrum thus corresponds with a ratio between CW and CCW powers in the disk of 8 dB . Moreover, in Fig. 9 (top) there is a clear lasing threshold visible just above 0.5 mA for the CW curve, but not for the CCW curve.

It has been shown in [9] that the degree of unidirectionality (the ratio of the powers in the two directions $P_{\text{CW}}/P_{\text{CCW}}$) at low bias (power) levels is simply given by the ratio of the coupling coefficients $|K_1/K_2|$ with K_1 and K_2 the coupling from CCW to CW and vice versa. These coupling coefficients take into account both distributed coupling (e.g., due to scattering at sidewall surface roughness) and coupling due to discrete reflections (at Bragg gratings, facets, etc.). It has been shown in [7] that information about the coupling coefficients can be derived from the relative intensity noise (RIN) spectra of the microdisk laser.

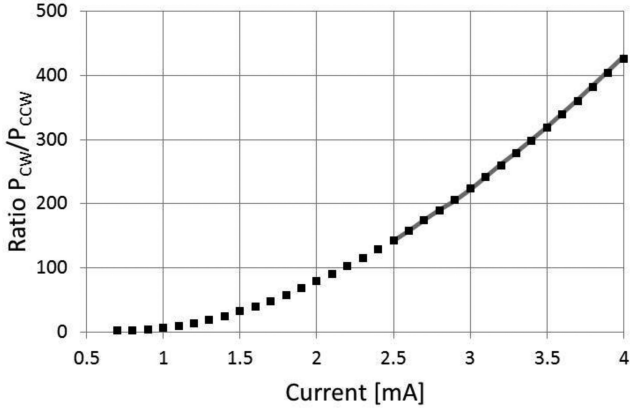


Fig. 10. Ratio of power in CW and CCW modes, (■) obtained from a numerical solution of the coupled rate equations, for a microdisk laser with coupling coefficients $K_1 = 6.36 \times 10^8 \text{ s}^{-1}$, $K_2 = 3.18 \times 10^8 \text{ s}^{-1}$, and (—) obtained from expression (23). $\varepsilon = 10^{-18} \text{ cm}^3$.

At high power levels however, unidirectional operation is significantly enhanced by the gain suppression or, more exact, the fact that the cross gain suppression is twice the self gain suppression. The ratio of the powers P_{CW}/P_{CCW} then approaches:

$$\frac{P_{CW}}{P_{CCW}} \approx \frac{\varepsilon G_0 P_{CW}}{2|K_2|} \quad (1)$$

with G_0 the threshold gain (per unit time), εP_{CW} the self gain suppression for the dominant mode and K_2 the smallest of the coupling coefficients (also per unit time).

Fig. 10 shows P_{CW}/P_{CCW} obtained from a time domain numerical solution of the coupled wave equations up to higher current levels for the case, $K_1 = 6.36 \times 10^8 \text{ s}^{-1}$, $K_2 = 3.18 \times 10^8 \text{ s}^{-1}$, and $\varepsilon = 10^{-18} \text{ cm}^3$ as well as the results for currents above 2.5 mA obtained using expression (1). Although the ratio K_1/K_2 is only 2, one obtains much higher P_{CW}/P_{CCW} values and they correspond quite well to the values obtained using (1).

The unidirectional behaviour can also lead to a lower sensitivity to external reflections, especially in the high power regime. If a microdisk laser (or ring laser) is lasing in a unidirectional mode, external reflections do not couple back or couple only weakly into the lasing mode. The ideal case is having no scattering within the disk and the bus waveguide having a perfectly AR-coated facet on one side and a low reflection at the other side.

We derive the feedback sensitivity from the change in angular frequency $\Delta\omega$ caused by the external reflection [31], [32]. For edge-emitting and vertical cavity surface emitting lasers, $\Delta\omega$ is traditionally expressed as [9]:

$$\Delta\omega = C\sqrt{1 + \alpha^2} \sin[\omega\tau_e + \arctg(\alpha)]r_e. \quad (2)$$

With r_e the external field reflection, C the feedback sensitivity, α the linewidth enhancement factor and τ_e the delay time of the external reflection.

The feedback sensitivity can always be reduced by increasing the laser facet reflectivities. This is however at the expense of the external efficiency η and it has even been shown that the feedback sensitivity C and the mirror loss α_{end} are proportional

[31]. For a Fabry–Perot laser with one 100% reflecting facet at the r.h.s. and a field reflection r_1 at the other (l.h.s.) facet, one can write:

$$|C| = \frac{2}{\tau_L} \alpha_{\text{end}} L \sqrt{K_z}$$

$$\frac{|C|\tau_L}{\alpha_{\text{end}}L} = \frac{1 - (r_1)^2}{-r_1 \ln(r_1)}. \quad (3)$$

With K_z the longitudinal Petermann factor and τ_L the roundtrip time in the Fabry–Perot laser cavity.

For an ideal microdisk laser without scattering inside the disk, a coupling κ between disk and bus waveguide and a field reflection r_1 at one facet and an undesired external reflection r_e at the other facet one can express $\Delta\omega$ as [9]:

$$\Delta\omega = r_e |C| \sqrt{1 + \alpha^2} \sin(\omega\tau_e + \arg(r_1) - \tan^{-1} \alpha)$$

$$\frac{|C|\tau_L}{\alpha_{\text{end}}L} = \frac{2\kappa^4}{-\ln(1 - \kappa^2)\tau_L} \frac{r_1}{\varepsilon G_0 P_{CW}}. \quad (4)$$

With r_1 the field reflection of the r.h.s. facet (or of the Bragg grating as in Fig. 8). r_1 can be chosen relatively small since it must just be larger than r_e to guarantee unidirectional operation at high output powers.

Since τ_L is typically of the order of ps or sub-ps, and $\varepsilon G_0 P_{CCW}$ is of the order of 10^{10} s^{-1} , the last factor in (4) is 100 or more. For values of κ^2 smaller than 1% and r_e smaller than 0.1, the normalized value of C can be smaller than that of an equivalent Fabry–Perot laser (with facet reflectivity R_1 larger than 99%). In both cases, the low feedback sensitivity is at the expense of the efficiency. The feedback sensitivity of microdisk lasers improves further with increasing power and decreasing r_1 though. The reflection sensitivity in this regime strongly depends on the gain suppression value. In our simulations and analytical approximations, we have taken a modest value for $\varepsilon = 10^{-18} \text{ cm}^3$, but much higher values have been reported in literature [33], [34], which give a much lower reflection sensitivity.

In general, with very low sidewall surface roughness, relatively high gain suppression values, low disk-bus coupling and if sufficiently high output powers can be reached, parasitic reflections should not pose a problem for optical interconnects using microdisk lasers.

IV. LOW POWER OPTICAL 2R REGENERATION

Ring and disk lasers have so far been used in the demonstration of a variety of nonlinear all-optical functions. This includes all-optical flip-flops [10], optical gates and wavelength converters, etc. Typical bitrates that can be handled are 10 to 20 Gb/s [3] and switching occurs with sub-pJ-pulses (1.8 fJ for AOFF, 160 fJ for gating) in times of 50 to 100 ps. All these optical switching functionalities require the input signal wavelength to be within the injection locking bandwidth of the laser or within the resonance bandwidth of the resonator (in case the microdisk is biased below threshold). In principle, the lasing or resonance wavelength of microdisk lasers can be thermally tuned with relatively lower tuning power [3] and the injection locking requirement is not a major drawback.

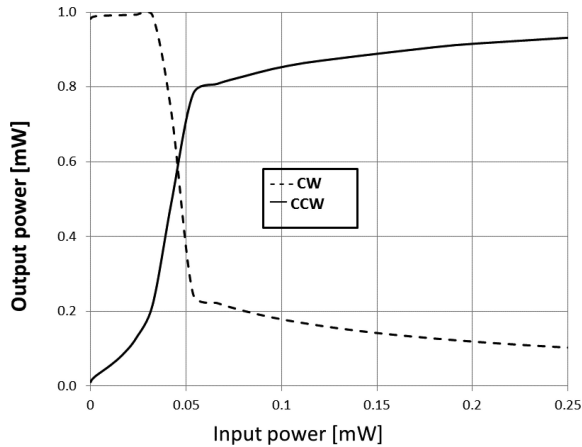


Fig. 11. Static regeneration characteristic for a microdisk laser with $K_2/K_1 = 10$.

Signal restoration or regeneration has been listed before (a.o. in [35]) as one of the key optical functionalities which must be possible in optical logic circuits. Regenerators show great promise for future large scale interconnect networks if the required optical input power and the device power consumption is lowered.

However, of the many all-optical regeneration schemes that have been reported in the past [36], [37], none were able to operate with very low input powers and with low power consumption.

We have recently presented an all-optical regeneration scheme based on asymmetric microdisk lasers that could operate with sub-mW input powers and with less than 10 mW of electrical power dissipation [38]. We will explain the scheme using Fig. 8, assuming R_1 to be larger than R_2 , and thus $|K_1/K_2| > 1$. The optical beam to be regenerated is injected from the low reflection side, i.e., from the left hand side. The regeneration scheme itself relies on the fact that an external signal within the injection-locking bandwidth of the laser, injected at the low reflection (or left hand) side, is equivalent to a reflection for the laser field at that side. If no or little light is injected from the left hand side, the equivalent $|K_1/K_2|$ will remain larger than one. The microdisk (or ring) laser will operate in the CW direction and little or no light will be coupled out from the right hand side. Injection of sufficiently high power at the left hand side (into the CCW direction) however will cause an equivalent reflection at the left hand side, which is larger than that at the right hand side and it will cause the equivalent $|K_1/K_2|$ to become smaller than one. The lasing direction will therefore switch from the CW to the CCW direction and a relatively high power will be coupled out from the right hand side. The threshold power for this switching obviously depends on the asymmetry of the microdisk laser and can be low for a small asymmetry. In this case, a sufficiently high bias will still give a good unidirectional behaviour, as discussed in part III.

Numerical simulations using a simple system of coupled rate equations show this threshold mechanism clearly. Fig. 11 shows the output power from the l.h.s. (CW) and r.h.s. (CCW) facets

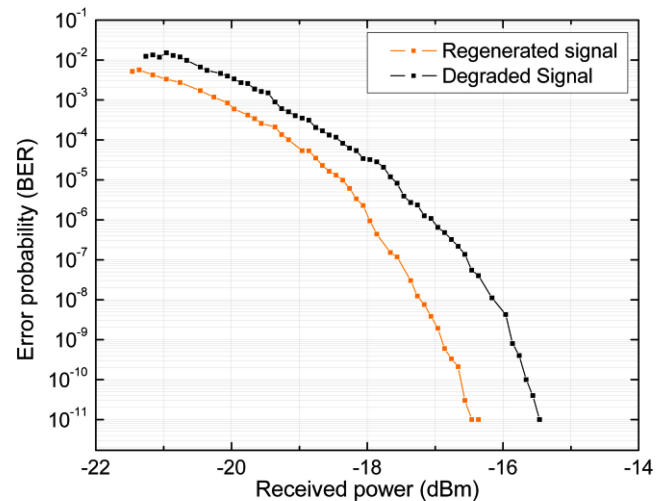


Fig. 12. Measured BER curves at 10 Gb/s, before and after regeneration with a microdisk laser.

respectively versus the input power injected at the l.h.s. facet. A distinct threshold and a relatively flat output power, ideal for regeneration, are obtained in the CCW mode. Dynamic simulations at 10 Gb/s have furthermore shown the possibility of extinction ratio improvement and noise reduction [38].

Experimentally, regeneration has been demonstrated for a 10 Gb/s NRZ signal (PRBS $2^{31} - 1$), which was attenuated and sent through an EDFA to degrade its signal-to-noise ratio. The measured BER before and after regeneration is given in Fig. 12 as a function of the received power. The microdisk laser was biased at 4mA and the experiments were carried out with relatively high extinction ratio (13 dB) for the input signal. Although the regeneration resulted in an output extinction ratio of 16 dB, Fig. 11 seems to indicate that even more extinction ratio and BER improvement can be obtained for lower input extinction ratio.

V. OPTICAL INTERCONNECT DEMONSTRATIONS

When using a heterogeneous integration approach, an obvious route towards optical interconnect on SOI is to use silicon waveguides and the same III-V layer stack for transmitter and detector [40]. However, MQWs are often preferred for the active layer of the laser and the small overlap of the optical mode with the quantum wells make this layer stack less suitable for the implementation of compact detectors. Another possibility is to use separate III-V dies for laser and detector, but they need to be spatially separated, which limits the integration density.

We proposed to use an epitaxial layer stack that contains both the laser and the detector epitaxy, with the detector layers stacked on top of the laser structure. This allows co-integrating detectors with lasers, as shown in Fig. 13. The detector epitaxial structure consists of a 100 nm n-doped InP layer, a 400 nm undoped InGaAs layer and a 100 nm heavily p-doped InGaAs layer. The transmitter epitaxial structure is similar to the one shown in Fig. 6(a). The n-doped InP layer acts both as top

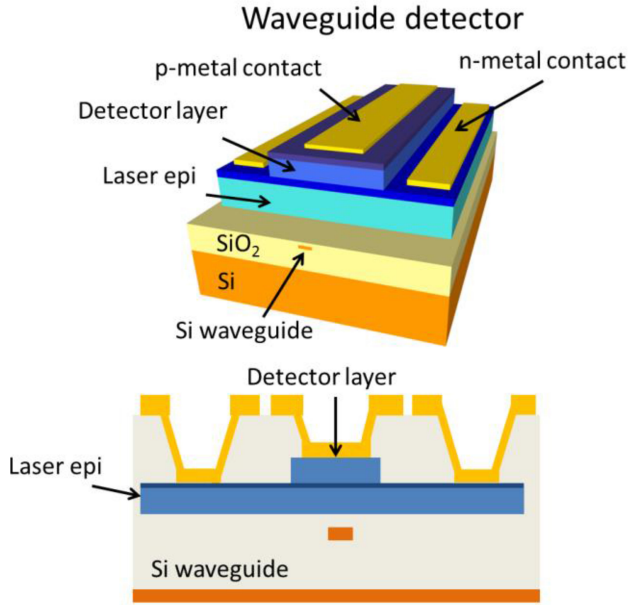


Fig. 13. Schematic overview of the detector design, where (a) shows a 3D impression and (b) shows the cross section of the detector.

contact layer for the microdisk laser and as bottom contact layer for the detector, making the total epitaxial layer stack 1083 nm thick.

As is the case for the coupling from microdisk laser to silicon waveguide, the coupling from silicon waveguide to the detector is through evanescent coupling. The bonding layer for optimum detection now needs to be as thin as possible though. On the other hand, the $1\ \mu\text{m}$ thick and several μm wide detector structure supports multiple optical modes, making it easier to achieve phase matching between the silicon waveguide and the detector waveguide. Simulations indicate that the coupling is mainly to the higher order modes of the detector waveguide. The silicon waveguide width (changed between 0.5 and $3\ \mu\text{m}$) did not affect the coupling very much, so $500\ \text{nm}$ wide waveguides were chosen for the fabrication.

Fabricated photodetectors of 40 and $60\ \mu\text{m}$ length gave dark currents (at a reverse bias of $1.5\ \text{V}$) of 22 and $67\ \text{nA}$. Responsivities were 0.69 and $0.73\ \text{A/W}$ respectively [41]. The dark current increases significantly with detector length due to the increased sidewall surface area, while the responsivity increase with length is marginal. A bandwidth of 12 and $18\ \text{GHz}$ was obtained for 0 and $-1\ \text{V}$ bias.

We have investigated two different link designs: a compact single link design with electrical contacts close to the devices for direct probing and a design containing multiple links, which can be driven by directly flip-chipping a CMOS control chip on top. Fig. 14 shows a current-current plot under pulsed driving conditions for the single link. Fig. 15 shows the large signal modulation response at $10\ \text{Gb/s}$ of the link. The direct modulation bandwidth of the microdisk laser was $7.8\ \text{GHz}$.

As an alternative for the III–V waveguide detector, one could of course also a Germanium detector [42]. Finally, direct modulation of microdisk lasers has been demonstrated at $20\ \text{Gb/s}$

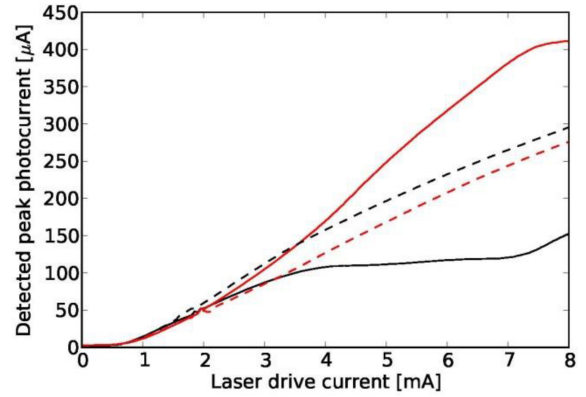


Fig. 14. Current versus current plot for two different optical links (dashed and solid lines) under pulsed drive conditions. The black and red curves correspond with the left and right detector, respectively.

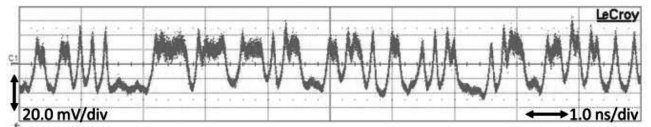


Fig. 15. Large signal modulation response of the full optical link for a $10\ \text{Gb/s}$ 2^7-1 PRBS pattern.

(using injection locking), with $1\ \text{mW}$ bias power and $190\ \text{mV}$ ($50\ \text{fJ/bit}$) data signals [43]. The low required drive voltages are compatible with standard CMOS logical levels. As discussed in [3], multi wavelength transmitters can be implemented by fabricating arrays of microdisks with different diameter, all coupled to the same bus waveguide. By providing InP heaters around the microdisks, thermal tuning of the lasing wavelength is possible with an efficiency of $0.3\ \text{nm per mW}$ of heating power [44].

VI. CONCLUSION

Recent developments in the fabrication and new applications of heterogeneously integrated microdisk lasers have been discussed. The bonding of the InP on the SOI occurs with high yield and with controllable thickness of the bonding layer(s). Improvements in processing have allowed achieving much better alignment accuracy, for both the disk with respect to the underlying silicon waveguide and for the top metal contact with respect to the center of the disks. Very good uniformity in lasing characteristics has been demonstrated as a result. A number of measures to reduce the losses for the whispering gallery mode and to improve the thermal behavior have been proposed as well.

Furthermore we have detailed how higher-efficiency, unidirectional lasing can be obtained from asymmetric microdisk lasers. At higher bias levels, such lasers can have a much lower external feedback sensitivity than traditional Fabry–Perot, DFB or DBR lasers or VCSELs. Moreover, they can be used as all-optical signal regenerators that operate on low input optical powers and with low power consumption.

Finally, optical interconnects on chip have been demonstrated at 10 Gb/s. An epitaxial layer stack that contains both the laser and the detector structure has been used for this purpose.

Further optimization in design and fabrication of the microdisk lasers could lead to further improvements in threshold current and output power as well as to reduced coupling between clockwise and counterclockwise modes. Such improvements would in turn make these lasers less sensitive to parasitic reflections, give higher modulation bandwidth and reduce electrical power consumption. They can also easily be operated in a predefined unidirectional mode, and several lasers with slightly different diameter and wavelength can be coupled to a single bus waveguide, thus forming a WDM source. Heterogeneously integrated microdisk lasers therefore could well turn out to be the ideal optical transmitters for silicon-based optical interconnects.

REFERENCES

- [1] P. R. Romeo *et al.*, "Heterogeneous integration of electrically driven microdisk based laser sources for optical interconnects and photonic ICs," *Opt. Exp.*, vol. 14, no. 9, pp. 3864–3871, 2006.
- [2] D. Liang *et al.*, "Optimization of hybrid silicon microring lasers," *IEEE Photon. J.*, vol. 3, no. 3, pp. 580–587, Jun. 2011.
- [3] D. Van Thourhout *et al.*, "Nanophotonic devices for optical interconnect," invited paper *IEEE J. Sel. Topics Quantum Electron.*, vol. 16, no. 5, pp. 1363–1375, Sep./Oct. 2010.
- [4] C. Gunn, "CMOS photonics for high-speed interconnects," *IEEE Micro*, vol. 26, no. 2, pp. 58–66, Mar./Apr. 2006.
- [5] S. Matsuo *et al.*, "Photonic crystal lasers using wavelength-scale embedded active region," *J. Appl. Phys. D*, vol. 47, no. 2, p. 023001, Jan. 2014.
- [6] M. Heck and J. Bowers, "Energy efficient and energy proportional optical interconnects for multi-core processors: Driving the need for on-chip sources," *IEEE J. Sel. Topics Quantum Electron.*, vol. 20, no. 4, art. no. 8201012, Jul./Aug. 2014.
- [7] G. Morthier and P. Mechet, "Theoretical analysis of unidirectional operation and reflection sensitivity of semiconductor ring or disk lasers," *IEEE J. Quantum. Electron.*, vol. 49, no. 12, pp. 1097–1101, Dec. 2013.
- [8] D. Liang *et al.*, "Teardrop reflector-assisted unidirectional hybrid silicon microring lasers," *IEEE Photon. Technol. Lett.*, vol. 24, no. 22, pp. 1988–1990, Nov. 2012.
- [9] P. Mechet *et al.*, "Unidirectional III-V microdisk lasers heterogeneously integrated on silicon," *Opt. Exp.*, vol. 21, no. 16, pp. 19339–19352, Aug. 2013.
- [10] L. Liu *et al.*, "An ultra-small, low-power, all-optical flip-flop memory on a silicon chip," *Nature Photon.*, vol. 4, pp. 182–187, 2010.
- [11] T. Spuesens, P. Regreny, and D. Van Thourhout, "Improved fabrication process for III-V based optical interconnects on silicon," in *Proc. IEEE 10th Int. Conf. Group IV Photon.*, 2013, pp. 154–155.
- [12] G. Mezosi, M. J. Strain, S. Furst, Z. Wang, and M. Sorel, "Unidirectional bistability in AlGaInAs microring and microdisk semiconductor lasers," *IEEE Photon. Technol. Lett.*, vol. 21, no. 2, pp. 88–90, Jan. 2009.
- [13] W. Wang, G. Yuan, G. Verschaffelt, J. Danckaert, and S. Yu, "Injection locking and switching operations of a novel retro-reflector-cavity-based semiconductor micro-ring laser," *IEEE Photon. Technol. Lett.*, vol. 20, no. 20, pp. 1673–1675, Oct. 2008.
- [14] R. Kumar *et al.*, "10 Gbit/s all-optical NRZ-OOK to RZ-OOK format conversion in an ultra-small III-V-on-silicon microdisk fabricated in a CMOS pilot line," *Opt. Exp.*, vol. 19, pp. 24647–24656, Nov. 2011.
- [15] J. Hofrichter *et al.*, "All-optical wavelength conversion using mode switching in an InP microdisc laser," *Electron. Lett.*, vol. 47, pp. 927–929, Aug. 2011.
- [16] A. Trita, G. Mezosi, M. Sorel, and G. Guiliani, "All-optical toggle flip-flop based on monolithic semiconductor ring laser," *IEEE Photon. Technol. Lett.*, vol. 26, no. 1, pp. 96–99, Jan. 2014.
- [17] S. Keyvaninia *et al.*, "Ultra-thin DVS-BCB adhesive bonding of III-V wafers, dies and multiple dies to a patterned silicon-on-insulator substrate," *Opt. Mater. Exp.*, vol. 3, no. 1, pp. 35–46, 2013.
- [18] P. Mechet *et al.*, "Uniformity of the lasing wavelength of heterogeneously integrated InP microdisk lasers on SOI," *Opt. Exp.*, vol. 21, no. 9, pp. 10622–10631, 2013.
- [19] J. Van Campenhout. (2007). Ph.D. dissertation, Ghent University. [Online]. Available: <http://photonics.intec.ugent.be/publications/phd.asp>.
- [20] T. Spuesens. (2014). Ph.D. dissertation, Ghent University. [Online]. Available: <http://photonics.intec.ugent.be/publications/phd.asp>.
- [21] M. Kostrzewa *et al.*, "InP dies transferred onto silicon substrate for optical interconnects application," *Sens. Actuators A, Phys.*, vol. 125, pp. 411–414, Jan. 2006.
- [22] D. Liang *et al.*, "High-quality 150 mm InP-to-silicon epitaxial transfer for silicon photonic integrated circuits," *Electrochem. Solid State Lett.*, vol. 12, pp. H101–H104, 2009.
- [23] G. Roelkens *et al.*, "Adhesive bonding of InP/InGaAsP dies to processed silicon-on-insulator wafers using DVS-bis-benzocyclobutene," *J. Electrochem. Soc.*, vol. 153, pp. G1015–G1019, 2006.
- [24] P. Mechet. (2014). Ph.D. dissertation, Ghent University. [Online]. Available: <http://photonics.intec.ugent.be/publications/phd.asp>.
- [25] S. Keyvaninia *et al.*, "Ultra-thin DVS-BCB adhesive bonding of III-V wafers, dies and multiple dies to a patterned silicon-on-insulator substrate," *Opt. Mat. Exp.*, vol. 3, pp. 35–36, 2013.
- [26] A. Bazin *et al.*, "Thermal improvement of InP wire photonic crystal laser on silicon by addition of diamond nanoparticles in polymer bonding layer," presented at the *36th Eur. Conf. Opt. Commun.*, Torino, Italy, 2010.
- [27] T. J. Karle *et al.*, "Heterogeneous integration and precise alignment of InP-based photonic crystal lasers to complementary metal-oxide semiconductor fabricated silicon-on-insulator wire waveguides," *J. Appl. Phys.*, vol. 107, art. no. 063103, 2010.
- [28] [Online]. Available: <http://inl.cnrs.fr/en/research-groups/item/26-heteroepitaxie-et-nanostructures>
- [29] M. Yamamoto, N. Yamamoto, and J. Nakano, "MOVPE growth of strained InAsP/InGaAsP quantum-well structures for low-threshold 1.3 μm lasers," *IEEE J. Quantum Electron.*, vol. 30, no. 2, pp. 554–561, Feb. 1994.
- [30] M. T. Hill *et al.*, "A fast low-power optical memory based on coupled micro-ring lasers," *Nature*, vol. 432, pp. 206–209, 2004.
- [31] O. Nilsson and J. Buus, "Linewidth and feedback sensitivity of semiconductor diode lasers," *IEEE J. Quantum Electron.*, vol. 26, no. 12, pp. 2039–2042, Dec. 1990.
- [32] R. Tkach and A. Chraplyvy, "Regimes of feedback effects in 1.5 μm distributed feedback lasers," *IEEE J. Lightw. Technol.*, vol. 4, no. 11, pp. 1655–1661, Nov. 1986.
- [33] A. Olivier *et al.*, "Determination of the gain compression coefficient of GaInAsP 1.5 μm multiple quantum well lasers by harmonic distortion measurements," presented at the *Opt. Fiber Commun.*, San Diego, CA, USA, 1991, p. 125.
- [34] J. Bowers, B. Hemenway, A. Gnauck, and D. Wilt, "High-speed constricted-mesa lasers," *IEEE J. Quantum. Electron.*, vol. 22, no. 6, pp. 833–844, Jun. 1986.
- [35] D. A. B. Miller and D. A. B. Miller, "Are optical transistors the next logical step?," *Nature Photon.*, vol. 4, pp. 3–5, 2010.
- [36] J. Leuthold *et al.*, "Novel 3R regenerator based on semiconductor optical amplifier delayed-interference configuration," *IEEE Photon. Technol. Lett.*, vol. 13, no. 8, pp. 860–862, Aug. 2001.
- [37] M. Rochette, L. B. Fu, V. Ta'eed, D. J. Moss, and B. J. Eggleton, 2R optical regeneration: An all-optical solution for BER improvement, *IEEE J. Sel. Topics Quantum Electron.*, vol. 12, no. 4, pp. 736–744, Jul./Aug. 2006.
- [38] P. Mechet *et al.*, "All-optical, low-power 2R regeneration of 10Gb/s NRZ signals using a III-V on SOI microdisk laser," presented at the 18th Optoelectron. Commun. Conf., 2014, Paper TuPO-4.
- [39] B. Li *et al.*, "Characterization of all-optical regeneration potential of a bistable semiconductor ring laser," *J. Lightw. Technol.*, vol. 27, no. 19, pp. 4233–4239, Oct. 2009.
- [40] G. Roelkens, D. Van Thourhout, R. Baets, R. Nötzel, and M. Smit, "Laser emission and photodetection in an InP/InGaAsP layer integrated on and coupled to a silicon-on-insulator waveguide circuit," *Opt. Exp.*, vol. 14, no. 18, pp. 8154–8159, Sep. 2006.
- [41] T. Spuesens *et al.*, "Compact integration of optical sources and detectors on SOI for optical interconnects fabricated in a 200 mm CMOS pilot line," *J. Lightw. Technol.*, vol. 30, no. 11, pp. 1764–1770, Jun. 2012.
- [42] L. Vivien *et al.*, "42 GHz p.i.n Germanium photodetector integrated in a silicon-on-insulator waveguide," *Opt. Exp.*, vol. 17, pp. 6252–6257, Apr. 2009.

- [43] O. Raz *et al.*, "50 fJ-per-bit, high speed, directly modulated light sources for on-chip optical data communications," presented at the Opt. Fiber Commun., Los Angeles, CA, USA, 2011.
- [44] L. Liu *et al.*, "A thermally tunable microdisk laser built on a III-V/silicon-on-insulator heterogeneous integration platform," *Photon. Technol. Lett.*, vol. 22, pp. 1270–1272, 2010.

Geert Morthier (M'93–SM'01) received the degree in electrical engineering and the Ph.D. degree from the University of Gent, Gent, Belgium, in 1987 and 1991, respectively. Since 1991, he has been a Member of the permanent staff of IMEC. His main research interests include the modelling and characterization of optoelectronic components. He has authored or coauthored more than 150 papers in the field and holds several patents. He is also one of the two authors of the *Handbook of Distributed Feedback Laser* (Artech House, 1997). From 1998 to end of 1999, he has been the Project Manager of the ACTS project ACTUAL dealing with the control of widely tunable laser diodes, from 2001 to 2005 he was Project Manager of the IST project NEWTON on new widely tunable lasers and from 2008 to 2011 he was Project Manager of the FP7 project HISTORIC on microdisk lasers. In 2001, he was appointed part time Professor at Ghent University, where he teaches courses on optical fiber communication and lasers.

He serves on the program committee of several international conferences

Thijs Spuesens received (S'08–M'08) received the M.Sc. degree in electrical engineering from the Eindhoven University of Technology, Eindhoven, The Netherlands, in 2008. In 2008 he joined the Photonics Research Group of Ghent University—imec, where he received the Ph.D. degree in photonics in 2014.

During his Ph.D. he was involved in the FP7 projects WADIMOS and HISTORIC, where he worked on the integration of III-V microsources and detectors on silicon for on-chip optical interconnects.

Currently he is involved in the FP7 project Plat4M, where he is working on platform development for silicon photonics.

Pauline Mechet received the B.Eng. degree in physics engineering, as well as the Engineer Diploma degree and the M.Sc. degree in optoelectronics from Grenoble I.N.P. PHELMA, Grenoble, France, in 2007 and 2009, respectively. In 2009, she joined the Photonics Research Group, Ghent University—IMEC, the Department of Information Technology. In 2014, she received the Ph.D. degree in photonics from Ghent University.

Her current research interests include heterogeneous integration of silicon-on-insulator and III–V materials and all-optical signal processing based on microdisk lasers.

Dr. Mechet is a Member of the IEEE Photonics Society.

Gunther Roelkens (M'02–SM'06) received the M.Sc. degree in electrical engineering in 2002 and the Ph.D. degree in electrical engineering in April 2007, both from Ghent University, Ghent, Belgium. He currently is a Tenure Track Professor at Ghent University working in the field of heterogeneously integrated silicon photonics waveguide circuits. He is also an Assistant Professor at the Eindhoven University of Technology, The Netherlands.

Dries Van Thourhout (M'00) received the Master's degree in physical engineering and the Ph.D. degree from Ghent University, Ghent, Belgium, in 1995 and 2000, respectively.

From October 2000 to September 2002, he was with Lucent Technologies, Bell Laboratories, Crawford Hill, NJ, USA, where he was engaged in InPInGaAsP monolithically integrated devices. In October 2002, he joined the Department of Information Technology, Ghent University, where he is involved in integrated optoelectronic devices. His current research interests include heterogeneous integration by wafer bonding, intrachip optical interconnect, and wavelength division multiplexing devices.